

**Chemical forms of calcium in Ca,Zn- and Ca,Cd-containing grains
excreted by tobacco trichomes**

Géraldine Sarret¹, Marie-Pierre Isaure, Matthew A. Marcus, Emiko Harada,
Yong-Eui Choi, Sébastien Pairis, Sirine Fakra and Alain Manceau

Géraldine Sarret, Marie-Pierre Isaure, Emiko Harada and Alain Manceau. Environmental Geochemistry Group, LGIT, University of Grenoble and CNRS, BP 53, 38041 Grenoble cedex 9, France

Matthew A. Marcus and Sirine Fakra. Advanced Light Source (ALS), Lawrence Berkeley National Lab, MS 6-100, Berkeley, CA 94720, USA

Emiko Harada and Yong-Eui Choi. Division of Forest Resources, College of Forest Sciences, Kangwon National University, Chunchon 200-701, Kangwon-do, Korea

Sébastien Pairis. Institut Néel CNRS-UJF, Dept. Matière Condensée, Matériaux et Fonctions, Pôle Instrumentation (Microscopie Electronique), 25 av. des Martyrs, BP 166, 38042 Grenoble cedex 9, France

¹ Corresponding author. Email: geraldine.sarret@ujf-grenoble.fr

Tel: (33) 4 76 82 80 21, Fax: (33) 4 76 82 81 01

1 **Abstract**

2

3 Tobacco (*Nicotiana tabacum* L. cv. Xanthi) plants exposed to toxic levels of zinc and cadmium
4 excrete metals through their leaf trichomes (epidermal hairs) as Zn,Ca- and Cd,Ca-containing
5 grains. Little is known about the nature and formation mechanism of these precipitates. The
6 chemical, crystalline, and non-crystalline compositions of individual grains produced by tobacco
7 were studied by scanning electron microscopy coupled with energy dispersive X-ray analysis
8 (SEM-EDX), micro-X-ray diffraction (μ XRD) and calcium K-edge micro X-ray absorption near
9 edge structure (μ XANES) spectroscopy. Zinc is predominantly incorporated in calcite, and
10 cadmium in calcite and vaterite. Aragonite, which occurs occasionally, does not seem to contain
11 trace metals. In addition to being precipitated in its three possible polymorphic forms, calcite,
12 aragonite and vaterite, calcium also is speciated as amorphous CaCO_3 and possibly organic Ca in
13 some grains. Most often, a particular grain consists of two or more crystalline and non-crystalline
14 phases. The observed variability of intra- and inter-grain elemental and phase composition
15 suggests that this biomineralization process is not constrained by biological factors, but instead
16 results from thermodynamically and kinetically controlled reactions. This study illustrates the
17 potential of laterally resolved X-ray synchrotron radiation techniques (μ XRD and μ XANES) to
18 study biomineralization and metal immobilization processes in plants.

19

20 **Keywords:** biomineralization, detoxification, micro-XANES, micro-XRD.

21 **Introduction**

22 Recently, a novel original mechanism of Zn and Cd detoxification was described in tobacco
23 (*Nicotiana tabacum* L. cv. Xanthi). Tobacco exposed to Cd excreted Cd,Ca-containing grains
24 through leaf trichomes (1, 2), and a similar excretion of Zn,Ca-containing grains was observed
25 under Zn exposure (3). Trichomes are specialized epidermal structures. In tobacco, they are
26 glandular and excrete various organic substances including nicotine and resins. Such
27 detoxification process may have implication in human health since smoking is one of the
28 principal routes of exposure to heavy metals, and also in phytoremediation as tobacco is a
29 candidate species for phytoextraction.

30 The morphology, elemental composition, mineralogy as well as Zn and Cd speciation in the
31 grains were investigated by scanning electron microscopy coupled with energy dispersive X-ray
32 analysis (SEM-EDX), micro-X-ray fluorescence (μ XRF), micro-X-ray diffraction (μ XRD), Zn
33 K-edge micro extended X-ray absorption fine structure (μ EXAFS) (3) and Cd L_{III} edge micro X-
34 ray absorption near edge structure (μ XANES) spectroscopy (Isaure et al., in prep.). Calcium was
35 always the major component. μ XRD analyses revealed the presence of calcite, and less
36 frequently vaterite and aragonite, two other CaCO₃ polymorphs. Calcium oxalate mono and
37 dihydrate were found occasionally. Calcite and vaterite were substituted by cations, probably Zn,
38 Cd and possibly Mn and Mg. Zn μ EXAFS confirmed the occurrence of Zn-substituted calcite,
39 and evidenced Zn associations with other phases including organic compounds, silica and
40 phosphate (3). Cd μ XANES showed that cadmium was a Ca substituent in calcite and vaterite
41 and/or sorbed on the surface of these minerals (Isaure et al., in prep.).

42 The mechanism of formation of these grains remains unclear. Biogenic minerals may result from
43 a controlled biomineralization process leading to well defined minerals and shapes. They may
44 also be “biologically induced”, which means that an organism promotes the precipitation, but
45 does not control the crystallization process (4). In the present case, grains could result from the
46 exudation of a liquid containing the various metals and substances, and precipitation of the
47 various solid phases due to water evaporation. Alternatively, they might be formed intracellularly
48 and excreted thereafter as suggested by Choi et al. (5). The purpose of this study is to better
49 characterize the structure and composition of the grains. Grains excreted by tobacco under
50 various Zn, Cd and Ca exposure conditions were investigated by SEM-EDX, μ XRD and Ca K-

51 edge μ XANES spectroscopy. Results of these complementary approaches are compared, and a
52 hypothesis for the formation of the grains is proposed in light of these data.

53

54 **Experimental**

55 *Materials*

56 Plant culture and grain collection procedure have been described previously (3). Briefly, tobacco
57 plants were grown in hydroponic conditions and exposed for 5 weeks to Zn or Cd, with or
58 without a supplement of Ca (Table 1). A control condition with Ca only was also tested. Then,
59 grains were collected by washing the leaves in ultrapure water and centrifugating the suspension.
60 Several Ca-containing reference compounds were used for the Ca XANES data analysis.

61 Calcite, vaterite and Cd-containing vaterite were synthesized at room temperature according to a
62 modified protocol of Paquette and Reeder (6, 7). Briefly, an aqueous solution (500 mL)
63 containing 10 mM CaCl_2 and 1.8 M NH_4Cl was placed in a glass reactor, an EPPENDORF tube
64 containing solid ammonium carbonate was allowed to float at the surface of the solution, and the
65 reactor was closed and kept unstirred. NH_4Cl was used as a background electrolyte to provide a
66 high ionic strength. Initial pH was 4.9. The decomposition of ammonium carbonate produces
67 $\text{NH}_3(\text{g})$ and $\text{CO}_2(\text{g})$, which dissolve into the solution, simultaneously increasing pH and
68 alkalinity. The supersaturation of the solution induces the formation and growth of CaCO_3
69 crystals. Continuous sublimation of $\text{NH}_3(\text{g})$ buffers the solution around $\text{pH} = 7.9$. After 13 days,
70 the reactor contained rhombohedral crystals and spherical particles attached on the surface of the
71 glass. The two types of particles were separated and characterized by XRD. Rhombohedral
72 crystals corresponded to calcite, and spherical particles to vaterite. For the synthesis of Cd-
73 containing vaterite, the same procedure was used except that after 13 days, when crystal size
74 amounted to 150-200 μm in diameter, the $\text{CaCl}_2\text{-NH}_4\text{Cl}$ solution was progressively doped with
75 0.1 M CdCl_2 to a total concentration of 100 μM Cd in order to incorporate Cd as a Ca substituent
76 in vaterite (6, 7). The progressive addition of CdCl_2 kept the solution undersaturated with respect
77 to otavite (CdCO_3). After 7 days, the particles were collected and separated. Spherical particles
78 were identified as Cd-containing vaterite by XRD and μXRF . The Cd content was a few tens
79 ppm based on μXRF analysis.

80 Aragonite was a natural specimen. The XANES spectrum for synthetic amorphous CaCO_3 was
81 provided by Y. Politi (8). Ca oxalate monohydrate (whewellite) was purchased from Aldrich. A

82 solution containing 0.5 M $\text{Ca}(\text{NO}_3)_2$ at pH 2.6 was used as a reference for aqueous Ca^{2+} . The
83 phase purity of all crystalline samples was checked by XRD prior to XANES analysis.

84

85 *Electron microscopy*

86 The morphology and the chemical composition of the grains were studied by SEM-EDX using a
87 Jeol-JSM 840A equipped with a Kevex Si(Li) detector. The chamber pressure was 10^{-6} - 10^{-5} Torr,
88 and the accelerating voltage 20 kV. Grains were mounted on kapton tape or on carbon tape, then
89 fixed on carbon stubs and coated with carbon. Images were taken at a magnification of 500 to
90 10000. EDX spectra were recorded on prominent spots of the grains to optimize the detection.

91

92 *Micro-XRF, μ XRD and μ XANES*

93 The μ XRF, μ XRD and Ca K-edge μ XANES measurements were performed on beamline 10.3.2
94 of the Advanced Light Source (ALS, Berkeley, CA) (9). The grains were spread on kapton tape
95 and analyzed at room temperature and pressure. First, each grain was mapped by μ XRF. Then,
96 μ XANES and μ XRD and data were recorded on the Zn-richest region for the Zn and Zn + Ca
97 treatments, on the Cd-richest region for the Cd and Cd + Ca treatment, and on the Ca-richest
98 region for the Ca treatment. μ XRF data were collected at 10 keV with a beam size of $5 \times 5 \mu\text{m}$.
99 The same X-ray spot size was used for Ca μ XANES. Fluorescence X-ray yield was measured
100 with a 7-element Ge solid-state detector. The spectra were recorded between 3900 to 4400 eV.
101 μ XRD patterns were recorded at an incident energy of 17 keV with a beam size of $16 \times 7 \mu\text{m}$.
102 More experimental details are given in (3). Ca XANES reference spectra were recorded at room
103 temperature on beamline ID21 at the European Synchrotron Radiation Facility (ESRF, Grenoble,
104 France). Each spectrum is the average of two to three spectra, each about 15 minutes long.

105

106 *XRD and XANES data treatment*

107 The XRD data treatment was performed as described previously (3). Briefly, after calibration with
108 alumina, two dimensional XRD patterns were integrated to one-dimensional patterns for peak
109 assignment. For substituted calcite crystals, the unit cell parameters a and c were refined, and the
110 stoichiometry of the substituent was estimated from these two parameters using the Vegard law
111 (10) with calcite, smithsonite (ZnCO_3) and otavite (CdCO_3) as end-members for the Ca-Zn and Ca-

112 Cd solid solutions. This approach cannot be used for substituted vaterite because of the absence of
113 a CdCO₃ structural analogue of vaterite.

114 XANES spectra were processed using WinXAS (11). All spectra were energy calibrated
115 with respect to calcite (inflection point for this reference set to 4042.6 eV). The collected scans
116 were averaged; background subtracted and normalized using linear (pre-edge) or cubic (post-
117 edge) polynomials. XANES spectra were then fitted by linear combinations using calcite,
118 aragonite, vaterite, Cd-containing vaterite, amorphous CaCO₃, aqueous Ca²⁺ and Ca oxalate
119 monohydrate reference spectra. The quality of the fits was quantified by the normalized sum-
120 squares residuals $NSS = \sum(\mu_{\text{experimental}} - \mu_{\text{fit}})^2 / \sum(\mu_{\text{experimental}})^2 \times 100$, in the 4000-4150 eV
121 range, where μ is the normalized absorbance. An energy shift of ± 0.5 eV maximum and a
122 correction of slope were allowed to account for the energy resolution of the monochromator and
123 for possible inconsistencies in data processing. For some spectra, linear combination (LC) fitting
124 did not provide satisfactory results, and over-absorption effects were suspected based on the
125 comparison of these spectra with the standards. Therefore, each spectrum was fitted with and
126 without a correction of over-absorption using a simple model (12). This model assumes that the
127 smooth part of the resonant absorption is a constant fraction of the non-resonant background
128 (which is a reasonable assumption in the XANES region) and that the sample is infinitely thick,
129 *i.e.*, totally absorbs the incident beam (which is probably true considering the energy range and
130 the size and global composition of the grains). The equation used is:

$$131 \quad y_{\text{experimental}} = (1 + a) / (1 + a \cdot y_{\text{corrected}}) \quad (1)$$

132 where y is the normalized resonant absorbance, which equals 0 below the edge and

133 oscillates around 1 above the edge, and $a = \mu_{\text{resonant}} / (\mu_{\text{non resonant}} + \mu_{\text{fluorescence}})$

134 where μ_{resonant} , $\mu_{\text{non resonant}}$ and $\mu_{\text{fluorescence}}$ are the three components of the absorbance μ .

135 Equation (1) can be solved as:

$$136 \quad y_{\text{corrected}} = y_{\text{experimental}} / (1 + a(1 - y_{\text{experimental}})) \quad (2)$$

137 The over-absorption parameter a equals 0 in the absence of over-absorption effect, and
138 increases with this effect. Because of the sample heterogeneity, the precise composition of the
139 sample is not known, so a is an adjusted parameter.

140

141 **Results**

142 The morphology of the grains as observed by SEM varied considerably. The grains varied from
143 10 μm to 150 μm in diameter. Each grain is an aggregate of different types of particles. The first
144 type is micro faceted crystallites (Insets in Fig. 1a and 1b) and the second type is globular
145 structures of various sizes (from 2 to 50 μm , Fig. 1c, 1d and 1e). Some grains such as Zn₂ (Fig.
146 1c) seem visually less crystalline. The elemental composition of the grains varies from one grain
147 to another, and within the same grain. Ca was always the major component regardless of the plant
148 metal treatment conditions. Minor elements include Mg, Si, P, Cl, K, and Zn or Cd depending on
149 the plant treatment (Fig. 1). The high Si peaks observed in Fig. 1a to 1d are attributed to kapton
150 tape on which the grains were mounted. Silicon is not detected in the grain presented in Fig. 1e
151 (mounted on carbon tape). However, Si was found in small amount in some grains (not presented
152 in this study), as well as Mn.

153 Our previous study using μXRD (3) showed that grain ZnCa₃ contained substituted calcite and
154 aragonite, that grain ZnCa₄ contained substituted calcite, and that grain Zn₂ did not contain
155 crystalline phases. The two-dimensional μXRD patterns for grains ZnCa₅ and Zn₃ show that the
156 Bragg reflections for these two grains consist of small arcs of Debye-Scherrer rings, indicating
157 that the grains are composed of micrometer-size mosaic crystals (Fig. 2b). All reflections
158 correspond to substituted calcite, and the major Ca substituent is Zn based on μXRF (Fig. 2a).
159 Note that although Ca is the major element, the Ca $K\alpha$ peak has a low intensity relative to the Zn
160 $K\alpha$ peak due to air absorption and the lower fluorescence yield of Ca *vs.* Zn. The refined unit cell
161 parameters *a* and *c* for grain ZnCa₅ and Zn₃ were 4.97 and 16.97 \AA , and 4.95 and 16.83 \AA ,
162 respectively, compared to 4.9896 and 17.0610 \AA for pure calcite. The calculated formulae using
163 the Vegard law were $\text{Ca}_{0.95}\text{Zn}_{0.05}\text{CO}_3$ and $\text{Ca}_{0.89}\text{Zn}_{0.11}\text{CO}_3$, respectively. The difference in the Zn
164 stoichiometry coefficient obtained using parameters *a* and *c* was ± 0.01 . The μXRD results for
165 the Cd-containing grains will be presented separately together with Cd L_{III} -XANES data (Isaure
166 et al., in preparation). Briefly, the grains CdCa₂ and Cd₁₀ contain micrometer crystals of
167 substituted calcite and finer (nanometer sized) crystals of substituted vaterite. Grain CdCa₃
168 contains nano-crystals of substituted vaterite only. Finally, no crystalline phases were detected in
169 grain CdCa₆. For Cd- substituted calcite, the Vegard law provides an imprecise estimation of Cd
170 stoichiometry because the contrast in ionic radius between Cd and Ca is small (0.95 \AA for Cd^{2+}
171 and 1.00 \AA for Ca^{2+} compared to 0.74 \AA for Zn^{2+}) (13). For instance, the substitution rate for
172 grain CdCa₂ could be anywhere between 30 and 80%. It was not possible to calculate the

173 stoichiometry of Cd in vaterite because of the absence of a Cd end member (see the Experimental
174 section).

175 Calcium being the major element in the grains, Ca K-edge μ XANES spectroscopy was then
176 performed to get some insights on the composition of the grains, and test for the presence of
177 amorphous Ca phases. Figure 3a shows the XANES spectra for several Ca reference compounds.
178 The four CaCO_3 species (calcite, vaterite, aragonite and amorphous CaCO_3 (ACC)) have clearly
179 distinct spectra, which enables their identification (14, 15). However, Ca XANES has no
180 sensitivity to substitutional impurities as seen for instance for low Cd-containing vaterite (Cd
181 content lower than 1%, as estimated by μ XRF) and pure vaterite exhibiting nearly identical
182 spectra. The spectra for aqueous Ca^{2+} , Ca oxalate monohydrate and ACC share some similarities.
183 However, the lower part of the edge is shifted to lower energy for ACC spectrum, and the
184 maximum of the white line (zero value of the first derivative) increases from 4049.5 eV (ACC) to
185 4049.9 eV (Ca oxalate monohydrate) and to 4050.5 eV (aqueous Ca^{2+} , Fig. 3b). The aragonite
186 spectrum is distinct from the three previous spectra in displaying a shoulder at 4046 eV (arrow in
187 Fig. 3), and a minimum between 4060 and 4070 eV.

188 Figure 4 shows the Ca μ XANES spectra for the grains. They were fitted by LC using the standard
189 spectra presented above, and results are presented in Table 2. The ZnCa3 spectrum presents
190 strong similarities with the aragonite spectrum, but markedly lower amplitude. The drop in
191 amplitude suggests some over-absorption effect (12) due to a high Ca content of the analyzed
192 spot. The fit without over-absorption correction (see materials and Methods) did not provide
193 satisfactory result ($NSS = 0.065$ %, with 68% vaterite + 25% aragonite). Introducing an over-
194 absorption correction greatly improved the fit ($NSS = 0.014$ % with aragonite as only component,
195 Fig. 4). The a value found (1.38) corresponds to a very strong over-absorption effect. The fit was
196 not improved significantly by introducing a second component (NSS decreased by less than
197 10%). Thus, the spot analyzed by μ XANES likely contains aragonite as the sole Ca species.
198 The grains ZnCa4 and ZnCa5 were fitted with 98% calcite. The fit was slightly improved with a
199 correction of over-absorption ($NSS = 0.015$ and 0.021 %, compared to 0.020 and 0.035 %, respectively),
200 and the proportions were unchanged. Adding a second component did not improve
201 significantly the fits (NSS decreased by less than 10%).

202 For grain Zn2 and CdCa6, fits without over-absorption correction were not satisfactory ($NSS =$
203 0.048 and 0.091 %, respectively, for two-component fits). Fair one-component fits with over-

204 absorption correction were obtained with ACC ($NSS = 0.021$ and 0.024 %, respectively), but the
205 match was not optimal for the first oscillation (around 4080 eV). Ca oxalate monohydrate and
206 aqueous Ca^{2+} provided weaker fits ($NSS = 0.086$ and 0.053 % for Zn2, and 0.076 and 0.043 % for
207 CdCa6, respectively). Adding a second component did improve the reproduction of the first
208 oscillation. Several fits of equivalent qualities were obtained with ACC as major component
209 (about 80 and 70 % of total Ca) and various species as secondary component. NSS values were
210 more than doubled if ACC was excluded (Table 2 and Fig. 1 in Supplemental Information).
211 Therefore, grains Zn2 and CdCa6 likely contain ACC as major species, and an additional species
212 whose nature remains unknown.

213 For the other grains (Zn3, CdCa2, CdCa3 and Cd10), over-absorption correction did not improve
214 the fits. Calcite was the major form in grains Zn3 and CdCa2, and fits of equivalent quality were
215 obtained with ACC, aqueous Ca^{2+} and Ca oxalate monohydrate as minor species. Aqueous Ca^{2+}
216 is unlikely in solid-state material. ACC and Ca oxalate monohydrate are more likely. In the
217 absence of reference spectra for Ca bound to organic ligands other than oxalate, this latter
218 compound may be considered as a proxy for Ca bound to organic compounds in general.
219 Therefore, this pool is referred to as “organic Ca and/or ACC” in Table 3. Vaterite was found in
220 grains CdCa3 and Cd10. For this latter grain only, no satisfactory fit was obtained with two
221 components ($NSS = 0.046$ %), so a third component was introduced. Again, a contribution of
222 organic Ca and/or ACC was found in grains CdCa3 and Cd10.

223
224 The speciation of Ca was then compared with the mineralogy and morphology of the grains
225 (Table 3). The percentages were rounded to the nearest ten for clarity. Except for two grains,
226 ZnCa3 and CdCa2, the same crystalline species were identified by μ XRD and Ca μ XANES. Zn-
227 substituted calcite and Cd-substituted vaterite were identified by μ XRD in grains ZnCa3 and
228 CdCa2, respectively, but not by Ca μ XANES spectroscopy. This difference likely results from
229 the larger beam size and higher penetration depth of X-rays in XRD measurements relative to
230 μ XANES ($16 \times 7 \mu\text{m}$ vs $5 \times 5 \mu\text{m}$, and a few tens of μm at 17 keV vs. a few μm at 4 keV). Thus,
231 XRD probes a different material volume than Ca μ XANES even when conducted on the same
232 spot.

233

234 **Discussion and Conclusion**

235 Results showed that beside crystalline calcium carbonates (calcite, vaterite and aragonite), the
236 tobacco grains contained ACC as well. Whewellite (Ca oxalate monohydrate) did show up in
237 some XANES fits, but its presence could not be firmly attested. Ca oxalate mono- and dihydrate
238 have several XRD peaks in common with calcite, but peaks at distinct positions as well. These
239 two minerals were positively identified by μ XRD in other tobacco grains based on the presence
240 of these specific peaks (3). In the present study, no such peaks were found on the XRD patterns.
241 However, it is still possible that coarse crystals of Ca oxalate mono or dihydrate are present but
242 produce non-specific peaks only, or that Bragg conditions were not met for these coarse crystals.
243 Therefore, the presence of Ca oxalate mono- and dihydrate cannot be ruled out. Other
244 undetermined organic ligands may also complex Ca. In addition, mixed mineral and organic Ca
245 compounds such as organic matter-containing calcite (16) may occur.

246 The Ca μ XANES analysis showed that strong over-absorption effects may take place and
247 decrease dramatically the amplitude of the spectra. We show that this effect is far from negligible
248 when identifying and quantifying Ca species. For instance, for grain ZnCa3, the uncorrected
249 spectrum was fitted by 68% vaterite + 25% aragonite, and the corrected spectrum was fitted with
250 100% aragonite. Note that the LCF without over-absorption correction was relatively bad, which
251 alerted us on the possibility of an over-absorption effect.

252 In the environment, ACC is thermodynamically unstable and rapidly transforms into vaterite and
253 then calcite (17). However, it is found as a stable compound in plants (e.g., cystoliths) and
254 animals (e.g., cuticle of crustaceans, spicules of ascidiae, granules in molluscs) (18). ACC is
255 probably stabilized by proteins, magnesium and phosphorus in these organisms (18). In our case,
256 Mg and P were found in the grains.

257 Biologically controlled biomineralization leads to well defined mineral species and shapes.
258 Here, the variety of morphologies and of CaCO₃ crystal structures, and their coexistence with
259 amorphous and possibly organic forms, supports the hypothesis of a biologically induced (as
260 opposed to biologically controlled) biomineralization. This study illustrates the potential of
261 microfocused X-ray techniques to study biomineralization processes, and strategies of metals
262 immobilization developed by plants to cope with metal toxicity.

263

264 **Acknowledgements**

265 We acknowledge the ALS (Berkeley, USA) and the ESRF (Grenoble, France) for the provision
266 of beamtime. We are grateful to Jean Susini and the staff of beamline ID21 at the ESRF for their
267 technical support during the experiment. The operations of the Advanced Light Source at
268 Lawrence Berkeley National Laboratory are supported by the Director, Office of Science, Office
269 of Basic Energy Sciences, Materials Sciences Division, of the US Department of Energy under
270 Contract No. DE-AC02-05CH11231. We acknowledge Y. Politi and S. Weiner for sharing the
271 ACC Ca XANES spectrum, and two anonymous reviewers.

References

1. Choi, Y. E., Harada, E., Wada, M., Tsuboi, H., Morita, Y., Kusano, T. & Sano, H. *Planta* **213**, 45-50 (2001).
2. Choi, Y. E., Harada, E., Kim, G. H., Yoon, E. S. & Sano, H. *J. Plant Biol.* **47**, 75-82 (2004).
3. Sarret, G., Harada, E., Choi, Y. E., Isaure, M. P., Geoffroy, N., Birschwilks, M., Clemens, S., Fakra, S., Marcus, M. A. & Manceau, A. *Plant Physiol.* **141**, 1021-1034 (2006).
4. Lowenstam, H. & Weiner, S. *On Biomineralization* (Oxford University Press, New York, Oxford, 1989).
5. Choi, Y. E. & Harada, E. *J. Plant Biol.* **48**, 113-119 (2005).
6. Paquette, J. & Reeder, R. J. *Geochim. Cosmochim. Acta* **59**, 735-749 (1995).
7. Reeder, R. J. *Geochim. Cosmochim. Acta* **60**, 1543-1552 (1996).
8. Politi, Y., Levi-Kalisman, Y., Raz, S., Wilt, F., Addadi, L., Weiner, S. & Sagi, I. *Adv. Funct. Mat.* **16**, 1289-1298 (2006).
9. Marcus, M. A., MacDowell, A. A., Celestre, R., Manceau, A., Miller, T., Padmore, H. A. & Sublett, R. E. *J. Synchrotron Rad.* **11**, 239-247 (2004).
10. West, A. *Solid State Chemistry and its Applications* (Wiley, New York, 1984).
11. Ressler, T. *J. Phys. IV* **7**, c2-269 (1997).
12. Manceau, A., Marcus, M. A. & Tamura, N. in *Applications of Synchrotron Radiation in Low-Temperature Geochemistry and Environmental Science* (eds. Fenter, P., Rivers, M., Sturchio, N. & Sutton, S.) 341-428 (Reviews in Mineralogy and Geochemistry, Mineralogical Society of America, Washington, DC., 2002).
13. Shannon, R. D. *Acta Crystallogr. A* **32**, 751-767 (1976).
14. Levi-Kalisman, Y., Raz, S., Weiner, S., Addadi, L. & Sagi, I. *Adv. Funct. Mat.* **12**, 43-48 (2002).
15. Pattanaik, S. *Nucl. Inst. Meth. Phys. Res. B* **229**, 367-374 (2005).
16. Phillips, B. L., Lee, Y. J. & Reeder, R. J. *Environ. Sci. & Technol.* **39**, 4533-4539 (2005).
17. Ogino, T., Suzuki, T. & Sawada, K. *J. Cryst. Growth* **100**, 159-67 (1990).
18. Weiner, S., Levi-Kalisman, Y., Raz, S. & Addadi, L. *Connective Tissue Research* **44 Suppl. 1**, 214-218 (2003).

Table 1. Tobacco culture conditions and name of the grains investigated

Treatment conditions	Cation Concentrations in the Nutrient Solution (mM)			Grain Names	Techniques and References				
	Ca	Zn	Cd		SEM-EDX	μ XRD	Zn μ EXAFS	Cd μ XANES	Ca μ XANES
Zn	0.28	0.25	0	Zn2	(3) and this paper	(3)	(3)	-	this paper
				Zn3	-	this paper	unpubl.	-	-
Zn + Ca	3.28	0.25	0	ZnCa3	(3) and this paper	(3)	(3)	-	this paper
				ZnCa4	(3) and this paper	(3)	(3)	-	this paper
				ZnCa5	-	this paper	unpubl.	-	this paper
Cd	0.28	$0.08 \cdot 10^{-3}$	0.025	Cd10	(a)	(a)	-	(a)	this paper
Cd + Ca	3.28	$0.08 \cdot 10^{-3}$	0.025	CdCa2	(a)	(a)	-	(a)	this paper
				CdCa3	(a)	(a)	-	(a)	this paper
				CdCa6	(a)	(a)	-	(a)	this paper
Ca	3.28	$0.08 \cdot 10^{-3}$	0	Ca3	this paper	-	-	-	-

(a) Isaure et al., in prep.

Table 2. Ca μ XANES Results

Treatment	Grain Name	a^1	Proportion of Ca species (%) Determined by Linear Combination Fitting the μ XANES Spectra					Sum	NSS (%) ²		
			Calcite	Vaterite	Aragonite	Amorphous CaCO ₃	Aqueous Ca ²⁺			Ca oxalate 1 H ₂ O	
Zn+Ca	ZnCa3	1.38			97 ± 2			97	0.014 ³		
	ZnCa4	0.12	98 ± 2					98	0.015 ³		
	ZnCa5	0.17	98 ± 2					98	0.021 ³		
Zn	Zn2	0.27			22 ± 10	76 ± 15			97	0.011 ³	
		0.27				77 ± 15		20 ± 15	97	0.016	
		0.27				79 ± 15	17 ± 15		96	0.019	
		0.42				(excluded)	55 ± 15	45 ± 15	100	0.050	
	Zn3			62 ± 5			29 ± 5			91	0.009 ³
				70 ± 5					22 ± 5	92	0.016
				71 ± 5				21 ± 5		92	0.018

Cd+Ca	CdCa2		85 ± 5		13 ± 5		98	0.012 ³
			87 ± 5			10 ± 5	97	0.014
			89 ± 5		9 ± 5		98	0.015
	CdCa3		77 ± 5		21 ± 7		98	0.031 ³
			79 ± 5			20 ± 7	99	0.036
			82 ± 5		16 ± 7		98	0.037
	CdCa6	0.38		74 ± 15		25 ± 15	99	0.015 ³
		0.42		68 ± 15	32 ± 15		100	0.019
		0.28		(excluded)	73 ± 15	25 ± 15	98	0.040
Cd	Cd10		29 ± 7	42 ± 8		25 ± 5	96	0.022 ³
			25 ± 7	37 ± 8		34 ± 5	96	0.025
			28 ± 7	42 ± 8		26 ± 5	96	0.028

¹ Coefficient of over-absorption. ² Residual between fit and experimental data $NSS = \frac{\sum(\mu_{\text{experimental}} - \mu_{\text{fit}})^2}{\sum(\mu_{\text{experimental}})^2} \times 100$ in the 4000-4150 eV range, where μ is the normalized absorbance. ³ Fit shown in Fig. 4. The error bars on the percentages correspond to the variation needed to increase *NSS* by 20%.

Table 3. Summary of the information obtained on each grain¹

Treatment	Grain Name	Ca Speciation (μXANES Results)¹	Mineralogy (μXRD Results)	Aspect of the Grain (SEM Results)
Zn+Ca	ZnCa3	100% aragonite	Aragonite, Zn-subst. calcite (Ca _{0.93} Zn _{0.07} CO ₃)	faceted
	ZnCa4	100% calcite	Zn-subst. calcite (Ca _{0.87} Zn _{0.13} CO ₃)	faceted
	ZnCa5	100% calcite	Zn-subst. calcite (Ca _{0.95} Zn _{0.05} CO ₃)	not observed
Zn	Zn2	80% ACC + 20% undetermined	No diffraction peaks	rounded
	Zn3	70% calcite + 30% organic Ca and/or ACC	Zn-subst. calcite (Ca _{0.89} Zn _{0.11} CO ₃)	not observed
Cd+Ca	CdCa2	90% calcite + 10% organic Ca and/or ACC	Cd-subst. calcite, Cd-subst. vaterite	not observed
	CdCa3	80% vaterite + 20% organic Ca and/or ACC	Cd-subst. vaterite	rounded
	CdCa6	70% ACC + 30% undetermined	No diffraction peaks	not observed
Cd	Cd10	30% calcite + 40% vaterite + 30% organic Ca and/or ACC	Cd-subst. calcite, Cd-subst. vaterite	rounded + faceted

¹The error bar on the percentages varies from 5 to 15% depending on the species (see Table 2)

Figure Captions

Figure 1: SEM imaging for the grains ZnCa₃ (a), ZnCa₄ (b) Zn₂ (c), CdCa₃ (d) and grain Ca₃ (e), and EDX analyses were performed on the spots marked by a black cross.

Figure 2: μ XRF spectrum (a) one- and two-dimensional μ XRD patterns (b) for grain ZnCa₅ and Zn₃. All XRD peaks were attributed to substituted calcite. The positions of three peaks for pure calcite are indicated by arrows.

Figure 3: Ca K-edge XANES spectra for the reference compounds used in the linear combination fits (a) and zoom on the main peak for aqueous Ca²⁺, Ca oxalate monohydrate and ACC (b).

Figure 4: Ca K-edge μ XANES spectra for the tobacco grains and corresponding linear combination fits. Five spectra (Zn₂, CdCa₆, ZnCa₃, ZnCa₅ and ZnCa₄) were corrected for over-absorption.

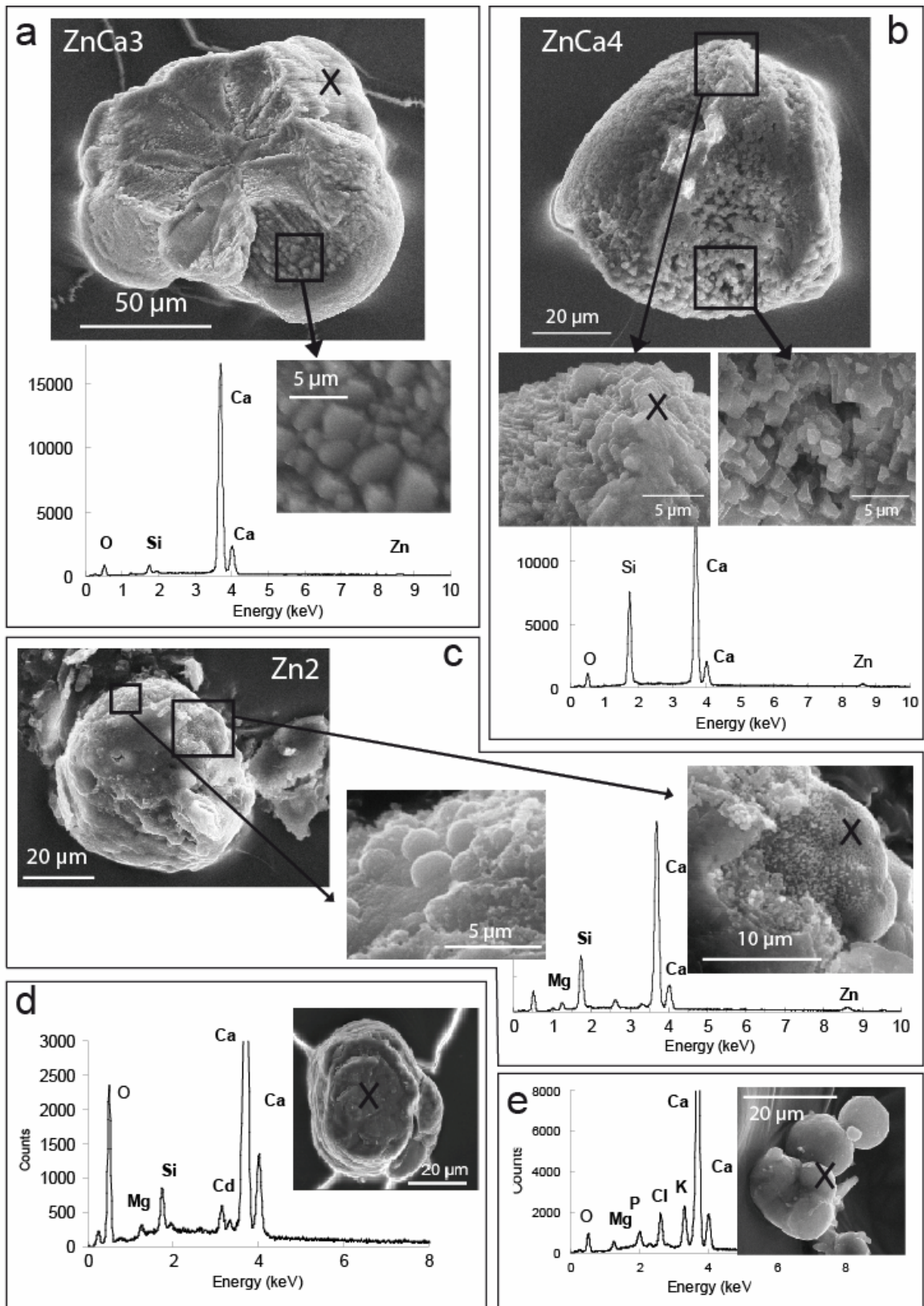


Figure 1

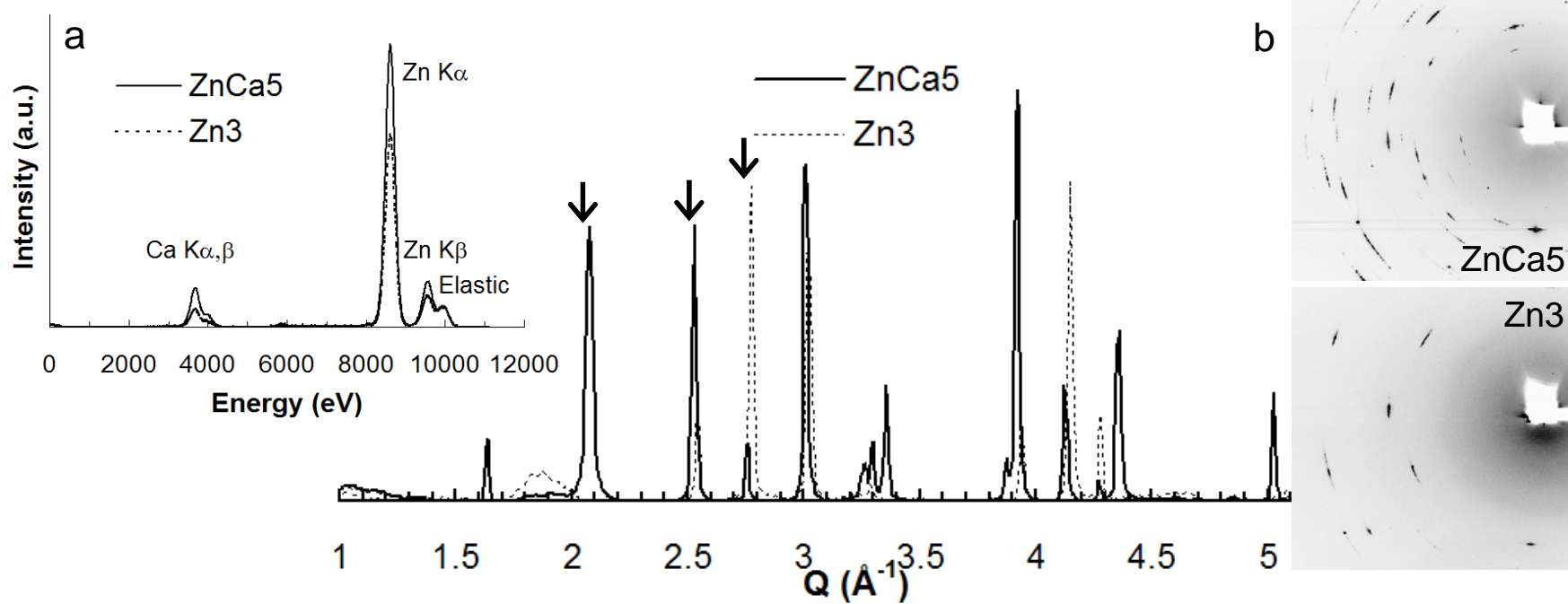


Figure 2

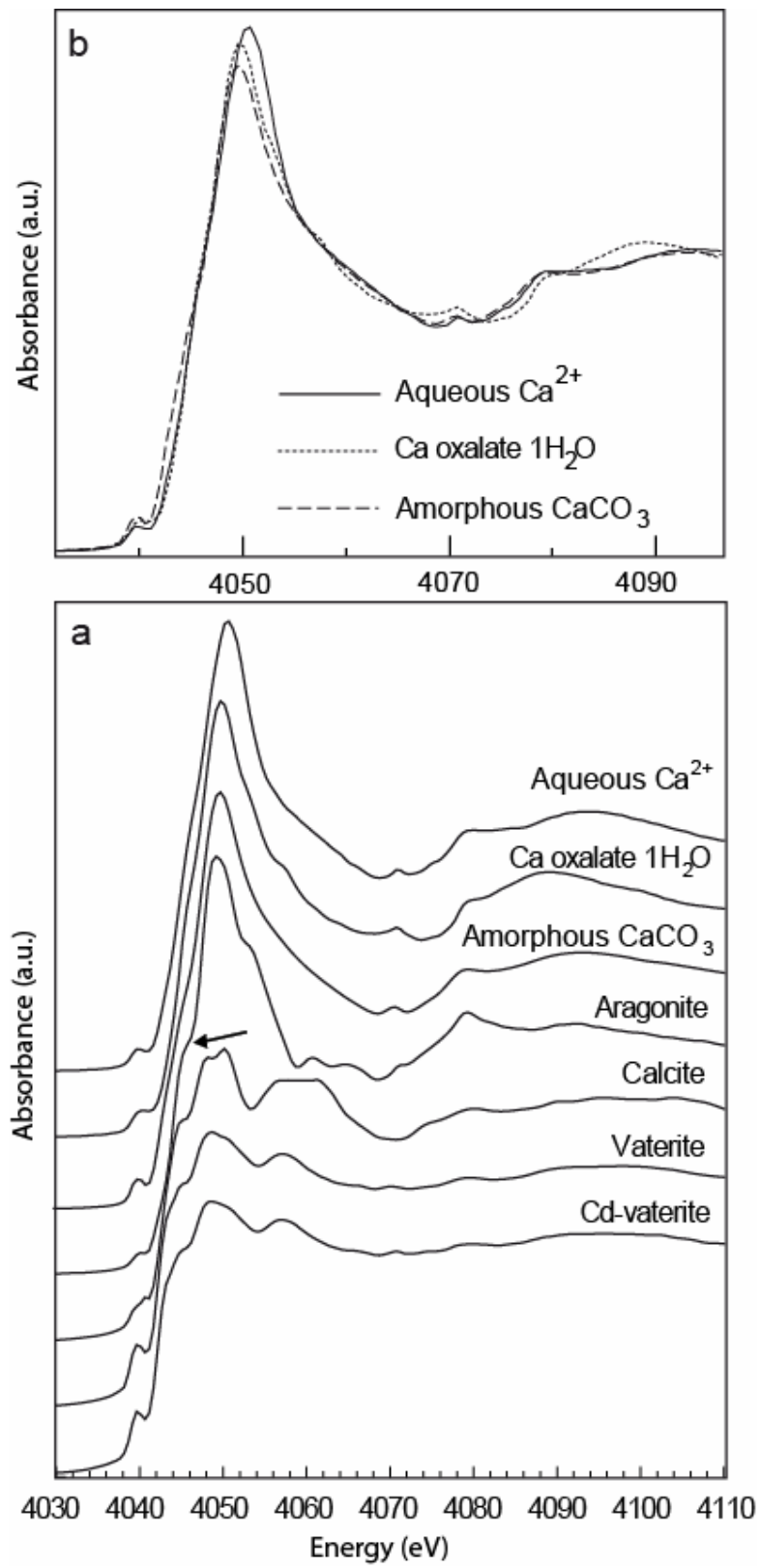


Figure 3

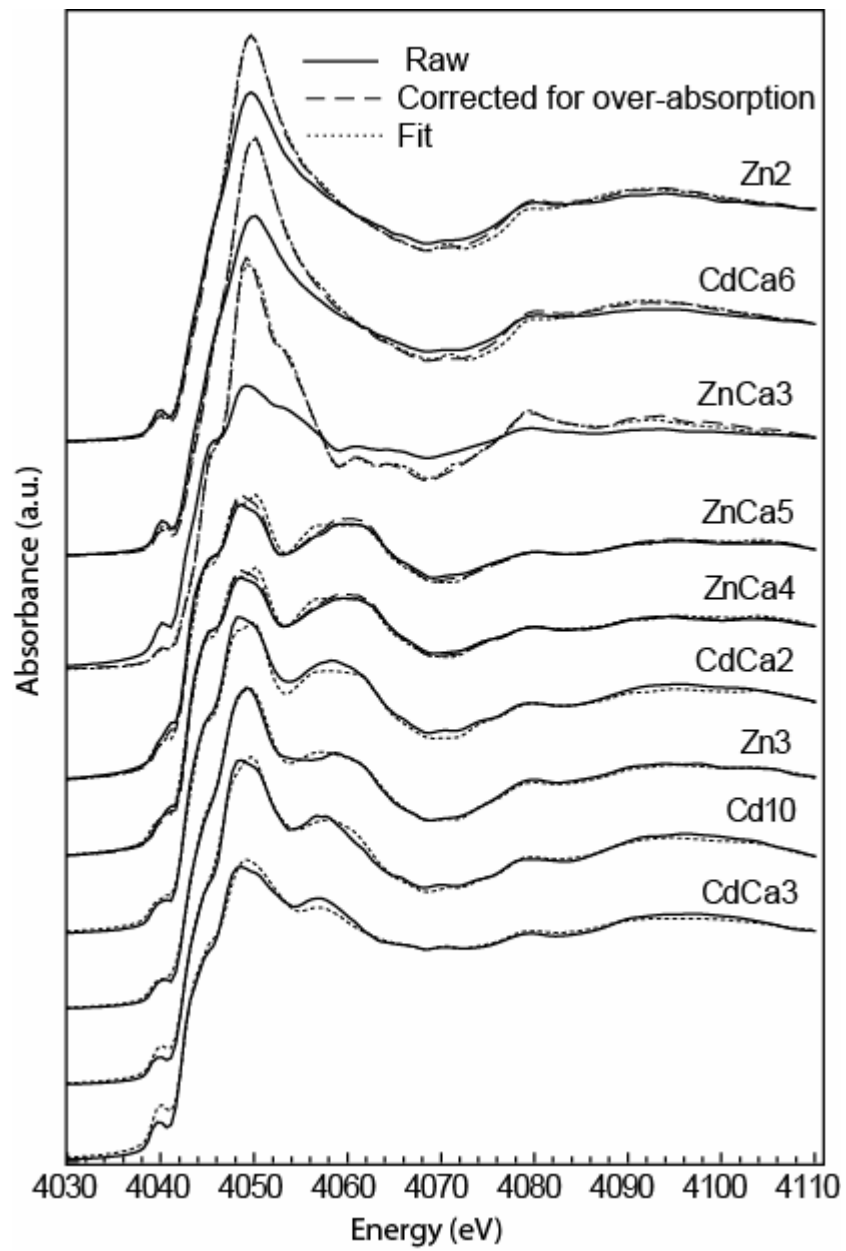


Figure 4

Supplemental information

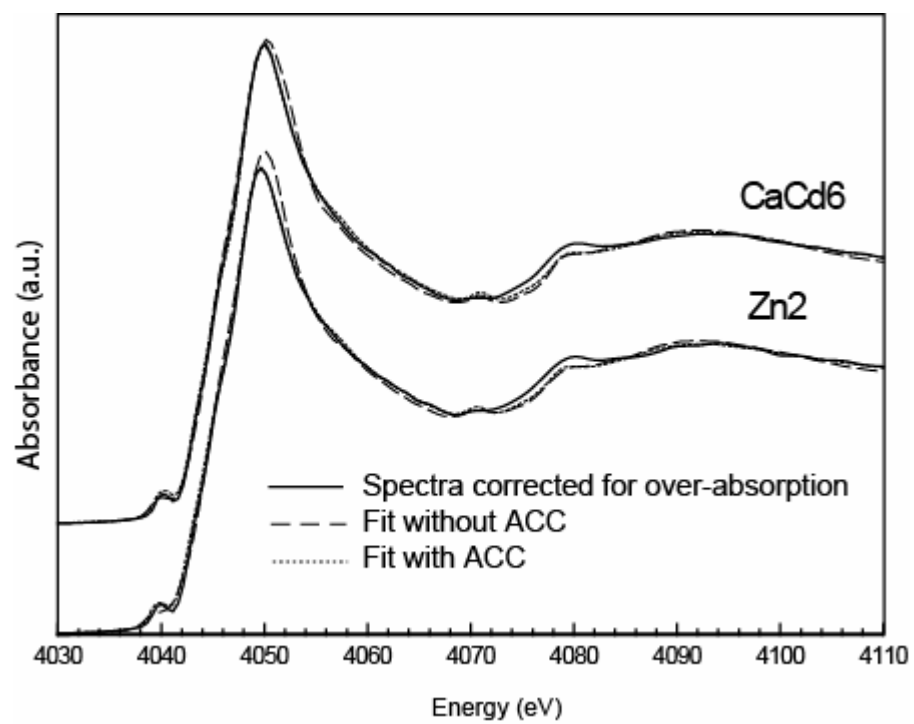


Figure 1: Comparison of the best two-component fits obtained for CaCd6 and Zn2 with and without ACC.